Thermal Properties of 12-Fold Quasi-Photonic Crystal Microcavity Laser With Size-Controlled Nano-Post for Electrical Driving

Wei-De Ho, Tsan-Wen Lu, Yi-Hua Hsiao, and Po-Tsung Lee, *Member, IEEE*

***Abstract*—In this report, we investigate the fabrication process of 12-fold quasi-photonic crystal microcavity with size-controlled nano-post beneath for electrically-driven structure by fine-tuning the wet-etching time. By finite-element method, we simulate and analyze the heat transfer behaviors of microcavities with different nano-post sizes and shapes. From the real devices, we obtain whispering-gallery (WG) single-mode lasing action with high measured quality factor of 8 250 and low threshold of 0.6 mW when the nano-post size is as large as 830 nm in diameter. By varying the substrate temperature, WG single-mode lasing action is still obtained when the substrate temperature is as high as 70°C. Besides, the lasing wavelength red-shift rate is also improved compared with the microcavity without nano-post beneath. By varying the pump condition, lasing action is still observed at room temperature when the pump duty cycle increases to 16.0%. Thus, for electrically-driven photonic crystal microcavity lasers, this nano-post can serve as current injection pathway and heat sink at the same time.**

***Index Terms*—Electrically-driven structure, microcavity, nano-post fabrications, photonic crystal, semiconductor laser.**

I. Introduction

SINCE the first demonstration by O. Painter *et al.* [1] in 1999, photonic crystal (PhC) microcavity lasers with high quality (Q) factor [2] and small mode volume [3] have been regarded as potential candidates in serving as highly efficient and low threshold light sources for photonic integrated circuits [4] and quantum electro-dynamics applications [5]. To promote PhC microcavity lasers into industrial applications, the electrically-driven structure is necessary. Typically, most present PhC microcavities are constructed based on a suspended slab in air to obtain good optical confinement in vertical direction, which leads to high Q factors. However, to build a pathway for highly efficient current injection on such suspended structure has long been an arduous task. Fortunately, this goal has been achieved very recently by inserting a central nano-post as a current pathway beneath the PhC microcavities, [6], [7] which is similar to the approach in electrically-driven micro-disk lasers [8]. Recently, the similar micro- and nano-post structures have also been widely adapted and investigated for the goal of electrical-driving in various PhC micro- and nano-cavity lasers by several groups [9]–[14]. In addition to the current pathway, the nano-post can also play the role of heat sink for the microcavity, which could be expected to provide the possibility of continuous-wave (CW) operation due to the improved heat dissipation. But this point has not been addressed and investigated in experiments yet.

In this nano-post structure, the sustained mode has to avoid the perturbation and degradation induced by the inserted nano-post. Thus, whispering-gallery (WG) mode will be a good candidate for the post structures due to its central zero field node. By proper design, high Q WG modes can be created or enhanced in various PhC based micro- and nano-cavities [13], [15]–[19]. In our previous report [13], we have investigated the WG modal behaviors in 12-fold quasi-PhC (QPhC) microcavity with different nano-post sizes, and obtained high measured Q factor of 8 400 from $\mathrm{WG}_{6,1}$ (the former and latter sub-numbers denote the azimuthal number and radial order of the WG mode) mode with effective nano-post size of 420 nm in diameter. In simulations, we also initially address the better thermal and electrical properties for microcavity with large central nano-post (post size ~800 nm in diameter) and the trade-off between Q factor and above properties. However, including the size-controlled nano-post fabrication process and improved thermal properties in experiments are not illustrated and investigated in details in our previous works.

In this report, at first, we demonstrate and illustrate the fabrication of 12-fold QPhC microcavities with size-controlled central nano-posts in details. And then we simulate the heat dissipation improvements due to different nano-post sizes and shapes by finite-element method (FEM). From real devices, we measure the improved $\mathrm{WG}_{6,1}$ mode lasing properties from microcavity with large central nano-post size of 830 nm in diameter. We also conclude the improved thermal properties according to the lasing actions under high substrate temperature and large pump duty cycle.

II. Fabrication Process of 12-Fold Quasi-Photonic Crystal Microcavity With Size-Controlled Nano-Post

The scheme of 12-fold QPhC D_2 microcavity with a central nano-post beneath is shown in Fig. 1. There are two reasons for applying 12-fold QPhCs. First, WG mode with central zero field distribution can be well-sustained in simple microcavity design based on 12-fold QPhCs, which is very suitable

Manuscript received June 22, 2009; revised August 19, 2009. First published September 01, 2009; current version published October 09, 2009. This work was supported by the National Science Council (NSC) of Taiwan under Contract Numbers NSC-98-2120-M-009-002 & NSC-98-2221-E-009-015-MY2.

The authors are with the Department of Photonics and Institute of Electro-Optical Engineering, National Chiao Tung University, Hsinchu 300, Taiwan (e-mail: hwd.di96g@nctu.edu.tw; ricky.eo94g@nctu.edu.tw; yihua26@gmail.com; potsung@mail.nctu.edu.tw).

Digital Object Identifier 10.1109/JLT.2009.2031501

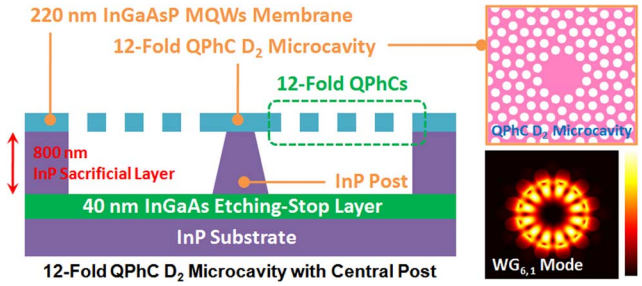

Fig. 1. Scheme of 12-fold QPhC D_2 microcavity with a nano-post beneath. The right insets show the microcavity geometry and the sustained high Q $\mathrm{WG}_{6,1}$ mode profile in electrical field, respectively.

for the nano-post structure. Secondly, the more isotropic photonic bandgap effect in different directions of 12-fold QPhC [20] than that of triangular PhC is good for WG mode with multi-pole resonance. The D_2 microcavity we investigate in this paper is defined by removing seven air-holes from QPhC lattice on a thin dielectric membrane with thickness and refrective index of 220 nm and 3.4. The simulated high Q $\mathrm{WG}_{6,1}$ mode profile with central zero electric-field node is also shown in the inset of Fig. 1. The simulated Q factor and filling factor of $\mathrm{WG}_{6,1}$ mode are 36 000 and 0.7, respectively, which are both beneficial to achieve low threshold laser source. The fabrication process starts from defining QPhC patterns by electron-beam lithography on polymethylmethacrylate on an epitaxial structure consisting of four compressively strained InGaAsP multi-quantum-wells (MQWs) with deposited $\mathrm{Si}_3\mathrm{N}_4$ hard mask. Then the QPhC patterns are transferred into MQWs by a series of reactive ion etching and inductively coupled plasma dry etching processes. Finally, the 800 nm InP sacrificial layer shown in Fig. 1 is opened up and the membrane microcavity with a central nano-post beneath is achieved by $\mathrm{HCl} : \mathrm{H_2O} = 3 : 1$ selective wet-etching process for 145 seconds. This wet-etching process also removes the $\mathrm{Si}_3\mathrm{N}_4$ hard mask residue. Top-, tilted-, and cross sectional-view scanning-electron-microscope (SEM) pictures of fabricated 12-fold QPhC D_2 microcavity with a central nano-post beneath are shown in Fig. 2(a). In Fig. 2(a), the fabricated nano-post can be identified from the white shadow in the top-view SEM picture or directly observed from the tilted-view SEM pictures. The fabricated lattice constant (a) and air-hole radius (r) over a (r/a) ratio are 520 nm and 0.34, respectively. The fabricated air-hole sidewall angle is estimated to be 87°. This can be further optimized to be 90° in fabrication to prevent unnecessary coupling losses to transverse-magnetic mode [21].

At the wet-etching step, to well control the nano-post formation, the temperature of diluted HCl solution is fixed at 2°C to slow down the InP etching rate, which is estimated to be 1.05 μm per minute along $\langle -1, 0, 0 \rangle$ direction of InP. And we define the effective nano-post size D as twice the distance from microcavity center to the outermost position occupied by the nano-post instead of the real size of nano-post, as shown in the left-most figure of Fig. 2(a). This is aimed at fairly estimating the influence on WG mode induced by the nano-post. In demonstrating the size-controlled nano-post, when we vary the wet-etching time from 110 to 160 seconds with r and lattice constant fixed at 190 and 520 nm, we observe the effective nano-post

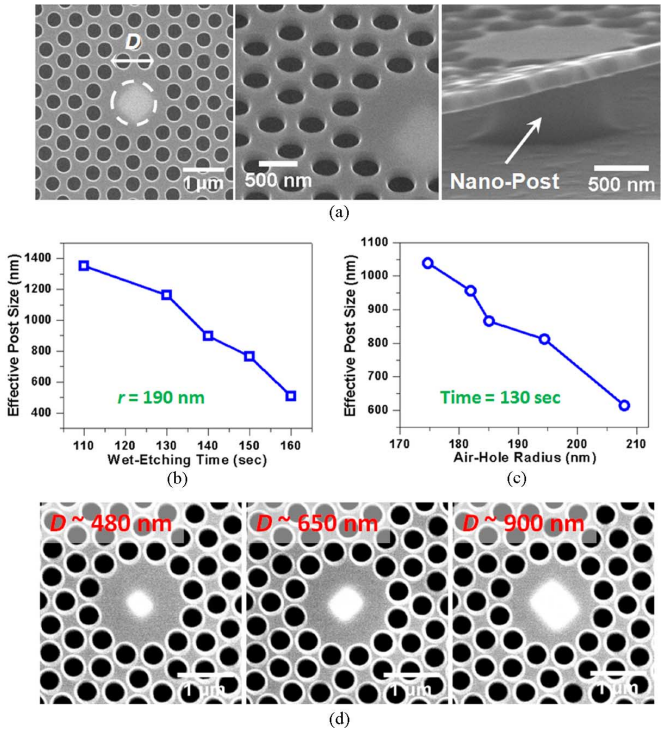

Fig. 2. (a) Top-, tilted-, and cross sectional-view SEM pictures of fabricated 12-fold QPhC D_2 microcavity with central nano-post beneath are shown from left to right. The nano-post beneath the microcavity can be easily identified and observed. (b) The relationship between nano-post size D and wet-etching time under fixed r. (c) The relationship between nano-post size D and air-hole radius r under fixed wet-etching time. (d) SEM pictures of fabricated 12-fold QPhC D_2 microcavities with different nano-post sizes $D = 480, 650$, and 900 nm by tuning the wet-etching time, from left to right.

size D varied from 1.4 μm to 500 nm, which is inverse-proportional to the wet-etching time, as shown in Fig. 2(b). On the other hand, when the wet-etching time is fixed at 130 seconds and the r is varied from 175 to 210 nm with the same lattice constant 520 nm, D is also inverse-proportional to the air-hole radius, as shown in Fig. 2(c). This is a reasonable relationship due to the loading effects of different air-hole sizes during the wet-etching process. The top-view SEM pictures of fabricated QPhC microcavities with nano-post sizes $D = 480, 650$, and 900 nm are shown in Fig. 2(d).

III. Simulated Heat Conduction Improvements due to Presence of Nano-Posts

To understand the role of nano-post in heat dissipation, we simulate the heat transfer behaviors of microcavities with different nano-post sizes by FEM. The details of 3-D FEM simulation setup can be found in our previous report [13]. In simulations, we merely consider the heat conduction that dominates the heat transfer behaviors. The model is given by:

$$\rho \times C \frac{\partial T}{\partial t} + \nabla \cdot (-k \nabla T) = H \tag{1}$$

where ρ, k, and C represent the density, thermal conductivity, and thermal capacity of material, respectively. The H denotes a time- and position-dependent surface heat source, which is an exponential decay form related to the absorption coefficient α

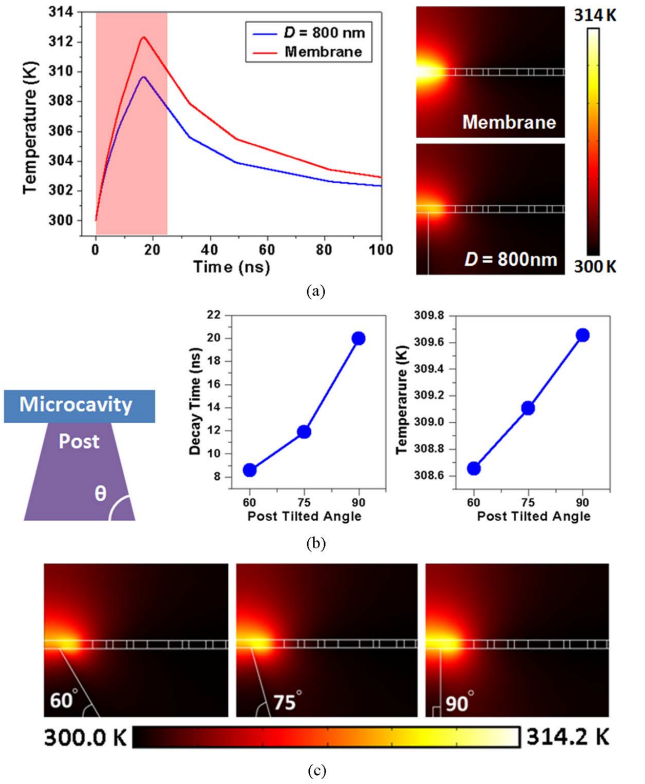

Fig. 3. (a) The simulated temperature decay curves of microcavities with nano-post sizes $D = 0$ (membrane without nano-post) and 800 nm. The corresponding simulated highest temperature distributions are also shown in the right insets. (b) From left to right: Illustraion of central nano-post with tilted angle θ beneath the microcavity and the plots of temperature decay time and highest temperature versus the nano-post tilted angle θ. (c) The simulated temperature distributions of microcavity with nano-post size $D = 800$ nm and tilted angles of 60°, 75°, and 90°.

($\sim 3.5 \times 10^6$ m^{-1}) of InGaAsP. The pulse width, duty cycle, energy level, and pump area of H are set to be 25 ns, 0.5%, 2 mW, and 2 μm in diameter, respectively, which are the typical values used in measurement. The simulated temprature decay curves of the microcavities with nano-post size $D = 800$ nm and membrane without nano-post ($D = 0$) are shown in Fig. 3(a). The highest temperature and decay time decrease from 312.4 to 308.7 K and from 25.3 to 20.0 ns when D is varied from 0 to 800 nm. The decay time is defined as the time duration for the temperature drop to $1/e$ of its highest value by first order exponential fitting after the pump source is turned-off. The time duration of pump source is indicated by the shadow region in Fig. 3(a). The simulated highest temperature distributions of $D = 0$ and 800 nm are also shown in the insets of Fig. 3(a). Above simulated heat transfer behaviors directly indicate that the nano-post beneath the microcavity can provide extra heat sink and improve heat dissipation.

In real situation, the nano-post formed under the microcavity is cone-shaped instead of a cylinder. This can be seen from the cross sectional-view SEM picture shown in Fig. 2(a). Therefore, the real nano-post volume will be larger than the cylinder nano-post with the same interface area (fixed D) connected to the membrane, which could contain more thermal energy. Thus, we simulate the heat transfer behaviors of microcavity with nano-post size $D = 800$ nm and tilted angles θ of 60°, 75° and 90°. The definition of θ is shown in Fig. 3(b). The simulated highest temperatures and decay times of cases with $\theta = 90°$, 75°, and 60° are 309.7, 309.1, and 308.7 K and 20.0, 11.9, and 8.6 ns, respectively, as shown in Fig. 3(b). From above results, we can conclude that the larger nano-post volume will provide better heat sink and improve heat dissipation.

In addition, we also calculate the electrical resistance by the formula of $R = \rho \times (L/A)$, where R, ρ, L, and A represent the electrical resistance, resistivity, height of nano-post, and the effective area (defined by the cross-sectional area at $L/2$ of the cone-shaped post) of the nano-post, respectively. The resistivity ρ of heavily Zn-doped ($\sim 10^{18}$ cm^{-3}) InP nano-post is 0.0417 $\Omega \cdot$ cm and L is fixed at 800 nm. The calculated R of nano-post size $D = 800$ nm and tilted angles of 60°, 75°, and 90° are 370, 621, and 1 043 Ω, respectively. Obviously, large nano-post volume will lead to low electrical resistance, which is beneficial in highly efficient current injection. Thus, to obtain improved thermal and electrical characteristics, the nano-post size D should be as large as possible. However, when D is larger than $1.6a$, the $\mathrm{WG}_{6,1}$ mode will be perturbed and the Q factor will degrade [13]. As a result, theoretically, under lattice constant of 520 nm, $D = 830$ nm is an upper limit when considering the trade-off between Q degradation, heat sink, and electrical resistance. In the following measurements, we will focus on the devices with large nano-post size $D \sim 830$ nm, where Q factor of $\mathrm{WG}_{6,1}$ mode still remains at 35 000 in FDTD simulations. High Q mode can lead to low threshold lasing action, which is beneficial for reducing unnecessary power input and the accompanied heat generation.

IV. Measured Modal and Thermal Properties

The 12-fold QPhC D_2 microcavities with nano-post size $D \sim 830$ nm are optically pumped at room temperature by an 845 nm diode laser with 25 ns pulsewidth and 0.5% duty cycle. We obtain $\mathrm{WG}_{6,1}$ single-mode lasing at 1485 nm. The measured light-in light-out (L-L) curve and lasing spectrum above threshold are shown in Fig. 4(a) and (b). The threshold is estimated to be 0.6 mW from the L-L curve. And the spectral line width is estimated to be 0.18 nm from the spectrum at 0.8 times threshold shown in the inset of Fig. 4(b) by Lorentzian fitting, which corresponds to a Q factor of 8 250. With large inserted nano-post, above lasing properties are significantly improved compared with those ($Q \sim 6\ 300$ and threshold $\sim$1.2 mW from the microcavity with similar nano-post size) we demonstrated before [13]. These are attributed to the improvements in our fabrication process, including the air-hole shape and sidewall angle, which both reduce unnecessary optical losses. When the nano-post size D increases, the $\mathrm{WG}_{6,1}$ mode suffers serious perturbation and lasing mode transition is observed. The measured spectrum of two lasing modes under transition when the nano-post size D is 1.1 μm is shown in Fig. 4(c). The lasing mode with shorter wavelength of 1420 nm is confirmed to be $\mathrm{WG}_{3,2}$ mode by finite-difference time-domain (FDTD) simulations. When the nano-post size further increases, the $\mathrm{WG}_{6,1}$ mode will be suppressed greatly, which leads to $\mathrm{WG}_{3,2}$ single-mode lasing. The FDTD simulated mode profiles of $\mathrm{WG}_{6,1}$ and $\mathrm{WG}_{3,2}$ modes in magnetic field are shown in

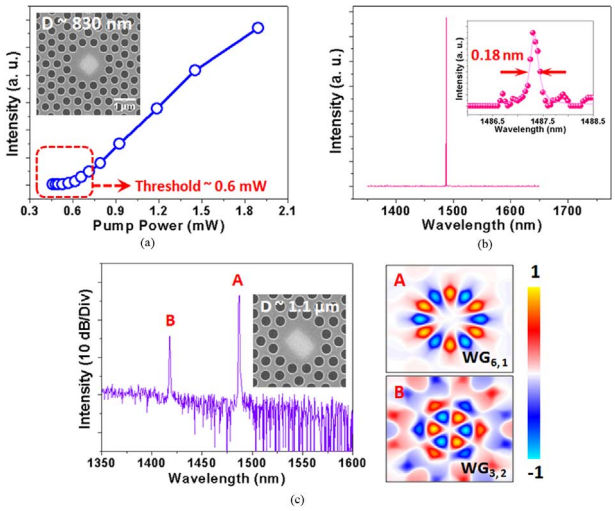

Fig. 4. (a) Typical L-L curve of 12-fold QPhC D_2 microcavity with nano-post size D of 830 nm. The threshold is estimated to be 0.6 mW and the SEM picture of measured device is also shown in the inset. (b) Typical spectra above and below threshold at wavelength of 1485 nm. The measured spectral line width below threshold is 0.18 nm by Lorentzian fitting. (c) The spectrum of $WG_{6,1}$ and $WG_{3,2}$ modes lasing when the nano-post size D increases to be 1.1 μm, as shown in the inset SEM picture. The FDTD simulated $WG_{6,1}$ and $WG_{3,2}$ mode profiles in magnetic field are also shown.

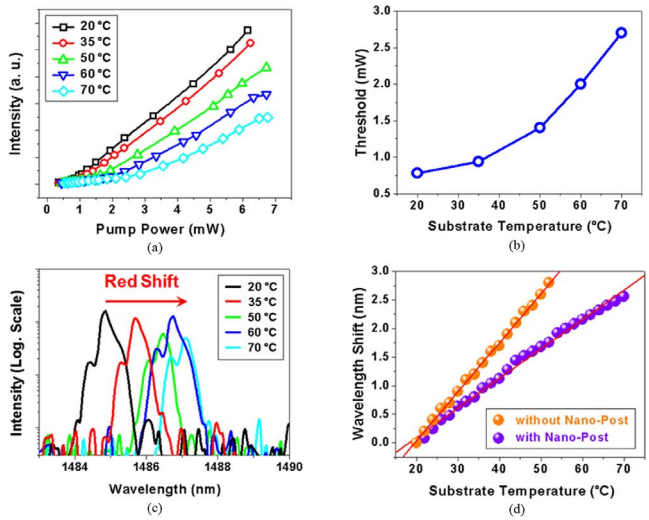

Fig. 5. (a) L-L curves of microcavity with nano-post size $D = 830$ nm under substrate temperatures of 20, 35, 50, 60, and 70°C, respectively. (b) The relationship between the threshold and the substrate temperature. (c) The red-shifted lasing spectra and (d) the lasing wavelength variation plot when the substrate temperature is varied from 20 to 70°C. The red-shift rate is about 0.050 nm/°C, which is smaller than that (0.086 nm/°C) of microcavity without nano-post beneath.

the insets of Fig. 4(c). Although the $WG_{3,2}$ mode field is more concentrated at the center of microcavity compared with $WG_{6,1}$ mode field, it will be enhanced by the micro-cylinder [22] effect when the enlarged nano-post size is larger than the mode field concentrated region.

To investigate the heat dissipation improvement provided by the nano-post, we change the substrate temperature of the microcavity with nano-post size $D = 830$ nm by a temperature controlling system. $WG_{6,1}$ single-mode lasing action can still be obtained when the substrate temperature is as high as 70°C, which is higher than the temperature limitation of 52°C from 12-fold QPhC D_2 microcavity without nano-post. This observed lasing action at high substrate temperature of 70°C is also better than those in PhC membrane microcavities with larger and similar microcavity sizes [23], [24], which can be attributed to the extra heat sink provided by the nano-post beneath. The measured L-L curves of $WG_{6,1}$ mode lasing when the substrate temperature is varied from 20 to 70°C are shown in Fig. 5(a). The threshold increases exponetially with the increased substrate temperature, as shown in Fig. 5(b). This is reasonable because there would be extra injected carrier wasting in non-radiative Auger and surface recombinations, which leads to the increase of threshold when the substrate temperature increases. The gain medium will also degrade with increased temperature, which in turn leads to the degraded slope efficiency. From Fig. 5(a), the decrease of slope efficiency monotonically with increasing substrate temperature also supports above argument.

We also observe the lasing wavelength red-shift when the substrate temperature increases from 20 to 70°C with 2°C increment, as shown in Fig. 5(c) and (d). We obtain total lasing wavelength red-shift of 2.5 nm, which corresponds to 0.050 nm/°C red-shift rate by linear fitting, as shown in Fig. 5(d). For comparison, we obtain the red-shift rate of 0.086 nm/°C from QPhC D_2 microcavity without nano-post as shown in Fig. 5(d), which is larger than 0.050 nm/°C of microcavity with nano-post under the same pump condition. Thus, we can conclude that the nano-post plays the role of heat sink and improves the heat dissipation indeed.

Due to the improved thermal properties obtained in experiments above, we then increase the duty cycle of pump source for the goal of CW operation. The measured L-L curves when the pump duty cycle is varied from 0.5 to 16.0% by changing pulsewidth with fixed repetition rate are shown in Fig. 6(a). When the pump duty cycle is increased to 8.0%, the threshold increases as shown in Fig. 6(a) and (b) but there is no significant change in slope efficiency compared with that when the pump duty cycle is 0.5%. However, when the pump duty cycle further increases to 16.0%, the threshold increases to 1.0 mW and the slope efficiency decreases significantly, as shown in Fig. 6(a). The increase of threshold and decrease of slope efficiency could be both attributed to the reasons of the degradations due to the increased temperature mentioned in the previous paragraph.

Besides, we also observe broadened spectral line width with increased pump duty cycle near threshold, as shown in Fig. 6(b) and (c), which directly indicates the increase of microcavity temperature with the increase of pump duty cycle. When the pump duty cycle further increases to 20.0%, the $WG_{6,1}$ mode lasing action is not always observed and the MQWs are destroyed when the pump duty cycle is larger than 20.0%. Although the CW operation is not available in this study, it is evident that the nano-post plays an efficient heat sink and improves the thermal performances of 12-fold QPhC D_2 microcavity. Thus, we still believe the CW operation can be obtained by this design with optimizations, for example, MQWs gain peak (near 1550 nm at room temperature) alignment with the microcavity resonance, improvement of fabrication imperfections, and so on.

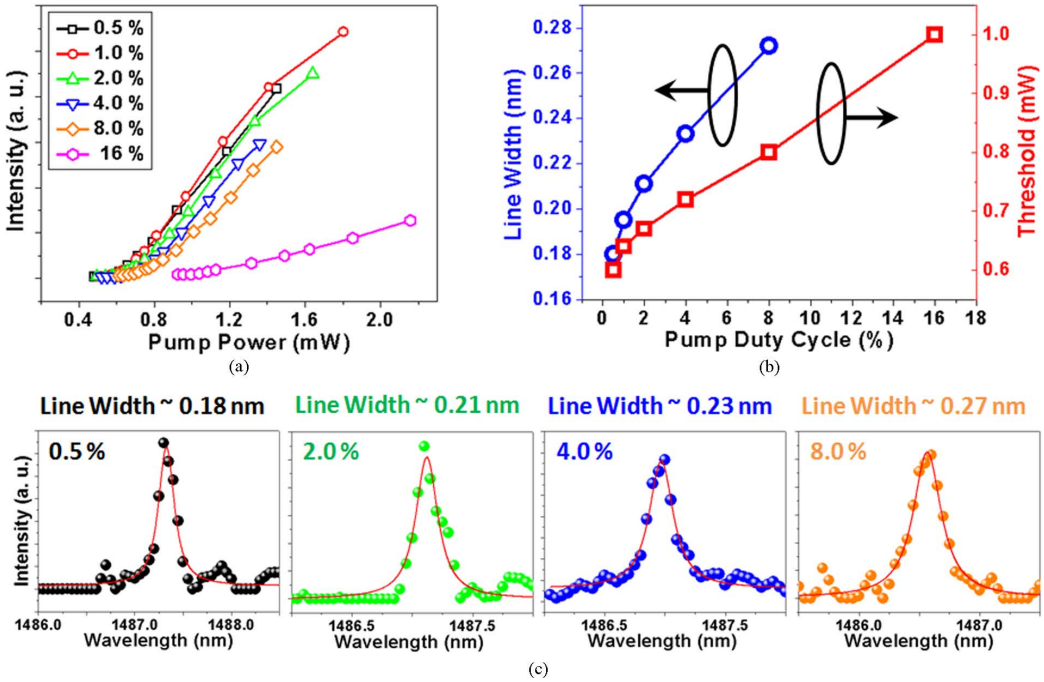

Fig. 6. (a) L-L curves of microcavity with nano-post beneath under different pump duty cycles from 0.5 to 16.0%. (b) The relationships of the pump duty cycle versus the spectral line width and the threshold. Both spectral line width and threshold increase with the increasing pump duty cycle. (c) The measured $\mathrm{WG}_{6,1}$ mode spectra below threshold when the pump duty cycles are 0.5, 2.0, 4.0, and 8.0%. The spectral line width is broadened due to the increasing thermal effect from the increased pump duty cycle.

Up to date, various excellent PhC nano- and micro-cavities operated in CW mode have been demonstrated [3], [25]–[28]. However, most of them still lack proper electrically-driven approaches. As a result, most importantly, based on this nano-post structure, we believe the realization of electrically-driven PhC microcavity laser under CW operation can be strongly expected. The nano-post can play the roles of current pathway and heat sink at the same time.

V. Conclusion

In conclusion, we introduce the fabrication process of 12-fold QPC D_2 microcavity with central nano-post beneath. The different nano-post size formations are investigated under conditions of varied r/a ratio with fixed wet-etching time and varied wet-etching time with fixed r/a ratio. According to these relationships, the size-controlled nano-post can be obtained by fine-tuning the wet-etching time with appropriate r/a ratio. To investigate and confirm the thermal performance improvement provided by the nano-post, by FEM simulation, we simulate the heat transfer behaviors of microcavities with different nano-post sizes D from 0 to 800 nm and shapes by different tilted angles θ from 90° to 60°. We can conclude that the microcavity with optimized nano-post size D as large as 800 nm and θ of 60° will provide better heat dissipation comparing with the membrane structure without Q degradation. In addition, we also calculate and show the large nano-post provides small electrical resistance. In measurements, from microcavity with nano-post size $D = 830$ nm, we obtain $\mathrm{WG}_{6,1}$ mode lasing at 1470 nm with high measured Q factor of 8 250 and low threshold of 0.6 mW, For experimental thermal characterizations, the $\mathrm{WG}_{6,1}$ mode lasing action from microcavity with nano-post size $D = 830$ nm is still observed when the substrate temperature is as high as 70°C. And we obtain the lasing wavelength red-shift rate of 0.050 nm/°C when varying the substrate temperature, which is better than 0.086 nm/°C from microcavity without nano-post beneath. Besides, the $\mathrm{WG}_{6,1}$ mode lasing action is still observed when the pump duty cycle is up to 16.0%. According to these results in simulations and experiments, we believe the realization of electrically-driven PhC microcavity laser under CW operation can be strongly expected based on this post structure, where the nano-post plays the roles of current pathway and heat sink at the same time.

Acknowledgment

The authors would like to thank the help from Center of Nano Science & Technology (CNST), National Chiao Tung University, Taiwan.

References

[1] O. Painter, P. K. Lee, A. Scherer, A. Yariv, J. D. O'Brien, P. D. Dapkus, and I. Kim, "Two-dimensional photonic bandgap defect mode laser," *Science*, vol. 284, pp. 1819–1821, 1999.

[2] Y. Takahashi, H. Hagino, Y. Tanaka, B. S. Song, T. Asano, and S. Noda, "High-Q nanocavity with a 2-ns photon lifetime," *Opt. Exp.*, vol. 15, pp. 17206–17213, 2007.

[3] K. Nozaki, S. Kita, and T. Baba, "Room temperature continuous wave operation and controlled spontaneous emission in ultrasmall photonic crystal nanolaser," *Opt. Exp.*, vol. 15, pp. 7506–7514, 2007.

[4] H. Park, A. Fang, S. Kodama, and J. Bowers, "Hybrid silicon evanescent laser fabricated with a silicon waveguide and III-V offset quantum wells," *Opt. Exp.*, vol. 13, pp. 9460–9464, 2005.

[5] K. Hennessy, A. Badolato, M. Winger, D. Gerace, M. Atatüre, S. Gulde, S. Fält, E. L. Hu, and A. Imaoğlu, "Quantum nature of a strongly coupled single quantum dot-cavity system," *Nature*, vol. 445, pp. 896–899, 2007.

[6] H. G. Park, S. H. Kim, S. H. Kwon, Y. G. Ju, J. K. Yang, J. H. Baek, S. B. Kim, and Y. H. Lee, "Electrically driven single-cell photonic crystal laser," *Science*, vol. 305, pp. 1444–1447, 2004.
[7] M. K. Seo, K. Y. Jeong, J. K. Yang, Y. H. Lee, H. G. Park, and S. B. Kim, "Low threshold current single-cell hexapole mode photonic crystal laser," *Appl. Phys. Lett.*, vol. 90, p. 171122, 2007.
[8] T. Baba, M. Fujita, A. Sakai, M. Kihara, and R. Watanabe, "Lasing characteristics of GaInAsP-InP strained quantum-well microdisk injection lasers with diameter of 2–10 μm," *IEEE Photon. Technol. Lett.*, vol. 9, no. 7, pp. 878–880, Jul. 1997.
[9] H. G. Park, S. K. Kim, S. H. Kwon, G. H. Kim, S. H. Kim, H. Y. Ryu, S. B. Kim, and Y. H. Lee, "Single-mode operation of two-dimensional photonic crystal laser with central post," *IEEE Photon. Technol. Lett.*, vol. 15, no. 10, pp. 1327–1329, Oct. 2003.
[10] S. Chakravarty, P. Bhattacharya, and Z. Mi, "Electrically injected quantum-dot photonic crystal microcavity light-emitting arrays with air-bridge contacts," *IEEE Photon. Technol. Lett.*, vol. 18, no. 24, pp. 2665–2667, Dec. 2006.
[11] L. Chen and E. Towe, "Design of high-Q microcavities for proposed two-dimensional electrically pumped photonic crystal lasers," *IEEE J. Sel. Topic. Quantum Electron.*, vol. 12, no. 1, pp. 117–123, Jan.-Feb. 2006.
[12] Z. H. Zhu, W. M. Ye, J. R. Ji, X. D. Yuan, and C. Zen, "Optimization for the high-Q monopole mode in electrically driven single-cell photonic crystal laser cavity," *J. Opt. Soc. Amer. B*, vol. 24, pp. 37–42, 2007.
[13] T. W. Lu, P. T. Lee, C. C. Tseng, and Y. Y. Tsai, "Modal properties and thermal behaviors of high quality factor quasi-photonic crystal microcavity," *Opt. Exp.*, vol. 16, pp. 12591–12598, 2008.
[14] Y. K. Kim, V. C. Elarde, C. M. Long, J. J. Coleman, and K. D. Choquette, "Electrically injected InGaAs/GaAs photonic crystal membrane light emitting microcavity with spatially localized gain," *J. Appl. Phys.*, vol. 104, p. 123103, 2008.
[15] H. G. Park, S. H. Kim, M. K. Seo, Y. G. Ju, S. B. Kim, and Y. H. Lee, "Characteristics of electrically driven two-dimensional photonic crystal lasers," *IEEE J. Quantum Electron.*, vol. 41, no. 9, pp. 1131–1141, Sep. 2005.
[16] H. Y. Ryu, J. K. Hwang, and Y. H. Lee, "The smallest possible whispering-gallery-like mode in the square lattice photonic-crystal slab single-defect cavity," *IEEE J. Quantum Electron.*, vol. 39, no. 2, pp. 314–322, Feb. 2003.
[17] P. T. Lee, T. W. Lu, J. H. Fan, and F. M. Tsai, "High quality factor microcavity lasers realized by circular photonic crystal with isotropic photonic bandgap effect," *Appl. Phys. Lett.*, vol. 90, p. 151125, 2007.
[18] H. Y. Ryu, M. Notomi, G. H. Kim, and Y. H. Lee, "High quality-factor whispering-gallery mode in the photonic crystal hexagonal disk cavity," *Opt. Exp.*, vol. 12, pp. 1708–1719, 2004.
[19] P. T. Lee, T. W. Lu, and F. M. Tsai, "Octagonal quasi-photonic crystal single-defect microcavity with whispering gallery mode and condensed device size," *IEEE Photon. Technol. Lett.*, vol. 19, no. 9, pp. 710–712, May 2007.
[20] M. E. Zoorob, M. D. B. Charlton, G. J. Parker, J. J. Baumberg, and M. C. Nett, "Complete photonic band-gaps in 12-fold symmetric quasicrystals," *Nature*, vol. 404, pp. 740–743, 2000.
[21] Y. Tanaka, T. Asano, Y. Akahane, B. S. Song, and S. Noda, "Theoretical investigation of a two-dimensional photonic crystal slab with truncated cone air holes," *Appl. Phys. Lett.*, vol. 82, pp. 1661–1663, 2003.
[22] Y. P. Rakovich, S. Balakrishnan, Y. Gun'ko, T. S. Perova, A. Moore, and J. F. Donegan, "Spontaneous emission enhancement in a microtube cavity with highly confined optical modes," in *Proc. SPIE*, 2007, vol. 6728, p. 672806.
[23] P. T. Lee, J. R. Cao, S. J. Choi, Z. J. Wei, J. D. O'Brien, and P. D. Dapkus, "Operation of photonic crystal membrane lasers above room temperature," *Appl. Phys. Lett.*, vol. 81, pp. 3311–3313, 2002.
[24] T. Yang, S. Lipson, J. D. O'Brien, and D. G. Deppe, "InAs quantum dot photonic crystal lasers and their temperature dependence," *IEEE Photon. Technol. Lett.*, vol. 17, no. 24, pp. 2244–2246, Nov. 2005.
[25] S. H. Kim, J. H. Choi, S. K. Lee, S. H. Kim, S. M. Yang, Y. H. Lee, C. Seassal, P. Regrency, and P. Viktorovitch, "Optofluidic integration of a photonic crystal nanolaser," *Opt. Exp.*, vol. 16, pp. 6515–6527, 2008.
[26] M. H. Shih, W. Kuang, T. Yang, M. Bagheri, Z. J. Wei, S. J. Choi, L. Lu, J. D. O'Brien, and P. D. Dapkus, "Experimental characterization of the optical loss of sapphire-bonded photonic crystal laser cavities," *IEEE Photon. Technol. Lett.*, vol. 18, no. 3, pp. 535–537, Feb. 2006.
[27] M. Nomura, S. Iwamoto, K. Watanabe, N. Kumagai, Y. Nakata, S. Ishida, and Y. Arakawa, "Room temperature continuous-wave lasing in photonic crystal nanocavity," *Opt. Exp.*, vol. 14, pp. 6308–6315, 2006.
[28] G. Vecchi, F. Raineri, I. Sagnes, A. Yacomotti, P. Monnier, T. J. Karle, K. H. Lee, R. Braive, L. Le Gratiet, S. Guilet, G. Beaudoin, A. Talneau, S. Bouchoule, A. Levenson, and R. Raj, "Continuous-wave operation of photonic band-edge laser near 1.55 μm on silicon wafer," *Opt. Exp.*, vol. 15, pp. 7551–7556, 2007.

Wei-De Ho received the B.S. degree from the Department of Engineering and System Science, National Tsing Hua University (NTHU), Hsinchu, Taiwan, in 2007 and the M. S. degree from the Display Institute, National Chiao Tung University (NCTU), Hsinchu, in 2009.

His research interests are focused on ion-based dry-etching technology developments and electrically-driven photonic crystal light emitters.

Tsan-Wen Lu received the B.S. degree from the Department of Electrical Engineering, National Tsing Hua University (NTHU), Hsinchu, Taiwan, in 2003 and the M.S. degree from the Institute of Electro-Optical Engineering, National Chiao Tung University (NCTU), Hsinchu, in 2005. In 2009, he received the Ph.D. degree in the Institute of Electro-Optical Engineering, NCTU.

His recent research interests are focused on III-V semiconductor-based photonic crystal microcavity laser and waveguide devices.

Yi-Hua Hsiao received the B.S. degree from the Department of Engineering Science, National Cheng Kung University (NCKU), Tainan, Taiwan, in 2007 and the M.S. degree from the Display Institute, National Chiao Tung University (NCTU), Hsinchu, Taiwan, in 2009.

His research interests are focused on electron-beam lithography technology developments and biosensor devices based on photonic crystal microcavities.

Po-Tsung Lee (M'06) received the B.S. degree from the Department of Physics, National Taiwan University (NTU), Taipei, Taiwan, in 1997 and the M.S. and Ph.D. degrees from the Department of Electrical Engineering-Electrophysics, University of Southern California (USC), Los Angeles, in 1998 and 2003, respectively. During the Ph.D. degree, she was engaged in photonic crystal microcavity lasers.

In 2003, she joined the Institute of Electro-Optical Engineering, National Chiao Tung University (NCTU), Hsinchu, Taiwan, as an Assistant Professor. In 2007, she became an Associate Professor in the Department of Photonics, NCTU. Her recent research interests are III-V semiconductor photonic crystal active and passive devices, electrical devices in display applications based on organic materials, and silicon-based solar-cell technologies.

Prof. Lee was the recipient of the University of Southern California Women in Science and Engineering (WISE) Award in 2000–2001.